KSCE Journal of Civil Engineering 29 (2025) 100163

Contents lists available at ScienceDirect

KSCE Journal of Civil Engineering

journal homepage: www.elsevier.com/locate/kscej

New computational platform of finite element reliability analysis for efficient safety assessment of bridges employing MIDAS/Civil

Seungjun Lee, Young-Joo Lee *

Dept. of Civil, Urban, Earth, and Environmental Engineering, Ulsan National Institute of Science and Technology (UNIST), Ulsan 44919, South Korea

ARTICLE INFO

Keywords:
Bridge
Finite element reliability analysis
FERUM
MIDAS/Civil
Computational platform

ABSTRACT

As the failure of bridges can cause significant damage to human life and property, the structural safety of bridges must be evaluated and monitored. In this study, a new computational platform that enables reliability analysis in conjunction with sophisticated finite element analysis for the risk-informed design and maintenance of bridges is proposed. In this regard, a software package for reliability analysis, i.e., Finite Element Reliability Using MATLAB (FERUM), is integrated with MIDAS/Civil, which is a widely-used commercial software package specialized for bridges. To control MIDAS/Civil during a reliability analysis, a control module of graphical user interface is added to FERUM. In addition, a recently-proposed algorithm is introduced in the developed platform to accurately locate the design points for reliability analysis based on the first-order reliability method. The accuracy and efficiency of the proposed method are compared with those of a sampling-based method via a numerical example, and the reliability-based safety of an actual bridge in the Republic of Korea is assessed for several vehicle load models. The new finite element reliability analysis platform is expected to enable efficient reliability-based evaluations of bridge safety.

1. Introduction

Bridges are important infrastructures and serve important functions in terms of transportation. Hence, the structural safety of bridges must be evaluated because bridge collapse can result in significant human and economic losses (Cook et al., 2015, Imam & Chryssanthopoulos, 2012). However, this is not a trivial task as various sources of uncertainty are associated with aging bridges, vehicle loads, and environmental conditions (Liu et al., 2023). Previously, structural safety was evaluated in a deterministic manner based on the assumption that the abovementioned factors have constant values; however, in recent decades, structural reliability analysis that considers the uncertainty of various influencing factors based on probability theory has been performed to assess the safety of bridge structures (Nowak & Szerszen, 2000, Tabsh & Nowak, 1991). Furthermore, this reliability analysis has been regarded as an important concept in terms of risk-informed bridge design and maintenance (Estes & Frangopol, 1999, Nowak, 1999, Fu, 2013).

In general, structural reliability analysis requires the calculation of the probability of an event when a structure reaches or exceeds a certain response level. Several structural reliability analysis methods have been developed and adopted to address various engineering challenges (Haldar, 2006). These challenges can be categorized into two groups based on the calculated probability: sampling-based and analytical (i.e., non-sampling-based) approaches. One of the representative methods of sampling-based approaches is the Monte Carlo simulation (MCS), which is widely used owing to its simple process for reliability analysis (Melchers, 2018). This method generally requires one to generate sufficient sets of random variables (RVs), conduct a structural analysis on each generated set, and verify whether the corresponding structural response exceeds a threshold value. In addition, for more accurate reliability analysis, a sophisticated structural analysis model (e.g., a finite element (FE) model) can be introduced into the MCS method (Lee & Moon, 2014). However, sampling-based approaches often require multiple structural analyses to achieve reliable results, and the introduction of sophisticated structural models and computationally expensive structural analyses (e.g., nonlinear structural analysis) may result in excessive time-consuming problems.

To overcome the disadvantages of simulation-based methods, many studies have been conducted to apply a non-sample-based method that performs a relatively small number of structural analyses but yields reliable results, which is often termed finite element reliability analysis (FERA). Since the attempt of Der Kiureghian and Taylor (Der Kiureghian

* Corresponding author.
E-mail addresses: sjlee5@unist.ac.kr (S. Lee), ylee@unist.ac.kr (Y.-J. Lee).

https://doi.org/10.1016/j.kscej.2025.100163
Received 30 June 2024; Received in revised form 25 November 2024; Accepted 17 January 2025
Available online 21 January 2025

& Taylor, 1983) in linking reliability and structural analysis algorithms, various structural reliability analysis software packages have been developed to perform structural reliability analysis accurately and efficiently. Software packages for structural reliability analysis can be classified into two types. The first type is reliability software that uses its own structural analysis modules, such as CalREL (Liu et al., 1989) and Finite Element Reliability Using MATLAB (FERUM) (Haukaas, 2003). These software packages do not require separate structural analysis software; however, they can be applied only to relatively simple structures (e.g., linear structural models) owing to the limitations of the built-in structural analysis software. Other types of structural reliability analysis software include NESSUS (SwRI, 2011), STRUREL (Gollwitzer et al., 2006), FERUM–ABAQUS (Lee et al., 2008, Kang et al., 2012), FERUM–ZEUS (Lee & Moon, 2014, Moon et al., 2018, Lee et al., 2021), and PIFA (Lee et al., 2016, Kim et al., 2017, Lee et al., 2019), which allow users to introduce sophisticated structural analysis methods to accurately represent structural behavior in structural reliability analysis. In particular, FERUM–ABAQUS, FERUM–ZEUS, and PIFA combine two software packages with different specializations to fully utilize their advantages in managing complex and diverse structural reliability problems.

Meanwhile, MIDAS/Civil (2020) is specialized software for bridge modeling and analysis, widely utilized in both practical applications and academic research. The software includes key features such as support for nonlinear analysis (Waseem & Spacone, 2017), time history analysis (Ho & Nishio, 2020), pushover analysis (Crespi et al., 2022), and staged construction analysis (Li et al., 2021), which enable users to examine the behavior of bridges under various loading conditions, including live loads (Hwang et al., 2013, Meng & Zhang, 2014, Park et al., 2018, Hwang & Kim, 2019), seismic loads (Huang et al., 2018), and wind loads (Zhang et al., 2022). Additionally, the software offers specialized tools for designing and analyzing composite girders (Shao et al., 2013), prestressed concrete (Lu et al., 2020), and cable-stayed (Lin et al., 2017) and suspension bridges (Cao et al., 2017). Furthermore, Midas/Civil facilitates the validation of theoretical models by integrating field measurements and experimental results (Xin et al., 2022, Zhang et al., 2022). Its intuitive interface and bridge-specific tools effectively support various tasks required for bridge design and safety assessments. However, despite its demonstrated effectiveness in various structural applications, Midas/Civil is less actively applied to probabilistic analysis compared to other FE analysis software, such as ABAQUS or ZEUS. This limitation arises from its reliance on a graphical user interface (GUI), which can restrict flexibility during reliability analysis.

In this study, FERUM–MIDAS, a new computational platform for FERA, is developed for the efficient safety assessment of bridges using MIDAS/Civil. By integrating FERUM with MIDAS/Civil, the developed platform allows for performing FERA while considering material nonlinearities in bridges and evaluating structural safety under various vehicle loading conditions. In the proposed platform, FERUM repeatedly calls MIDAS/Civil to perform structural analyses using various values of RVs, and the corresponding structural analysis results are returned to FERUM to conduct reliability analysis. Additionally, the recently proposed Hasofer–Lind and Rackwitz–Fiessler (HLRF)–Broyden–-Fletcher–Goldfarb–Shanno (BFGS) algorithm (Periçaro et al., 2015) is introduced in the developed platform to efficiently locate the first-order reliability method (FORM) design point. This integration provides a practical solution for incorporating probabilistic analysis into MIDAS/Civil, addressing a gap in its current application scope.

2. Reliability analysis method

Owing to its simplicity and efficiency, the FORM, which employs a linear approximation of the limit-state function (LSF) to estimate failure probability, has been widely adopted in various engineering problems (Haldar, 2006). The HLRF algorithm (Rackwitz & Flessler, 1978), specifically designed for this purpose, has proven to be efficient, although its robustness may be limited as it can indicate slow convergence or even fail to converge in the presence of highly nonlinear LSFs. In the study, an enhanced quasi-Newton approximation-based FORM (i.e., HLRF-BFGS) is implemented in FERUM to promote convergence in structural reliability analysis problems.

2.1. FORM

A LSF is typically defined to perform the reliability analysis of a structure. It is a mathematical representation of the behavior of a structure approaching a particular state. The LSF $g(\mathbf{x})$, which expresses the relationship between the resistance (R) and load (L) of the structure, can be written as

$$g(\mathbf{x}) = R(\mathbf{x}) - L(\mathbf{x}) \le 0 \tag{1}$$

where $\mathbf{x}$ is the vector of n RVs (i.e., $\mathrm{x} = [x_1, x_2, \ldots, x_n]^{\mathrm{T}}$) that describe the uncertainties in structural loads, material properties, and member geometry; $g(\mathbf{x}) \le 0$ typically indicates the failure of the structure. The failure probability, P_f, is then expressed as

$$P_f = P[g(\mathbf{x}) \le 0] = \int_{g(\mathbf{x})\le 0} f_{\mathbf{x}}(\mathbf{x})d\mathbf{x} \tag{2}$$

where $f_{\mathbf{x}}(\mathbf{x})$ is the joint probability density function (PDF) of the RV vector $\mathbf{x}$. Through the transformation of the space of the RVs into the standard normal space, P_f can be expressed as

$$P_f = \int_{g(\mathbf{x})\le 0} f_{\mathbf{x}}(\mathbf{x})d\mathbf{x} = \int_{G(\mathbf{u})\le 0} \varphi_n(\mathbf{u})d\mathbf{u} \tag{3}$$

where $G(\mathbf{u}) = g(\mathbf{T}^{-1}(\mathbf{u}))$ is the transformed LSF in the standard normal space, $\varphi_n(\cdot)$ denotes the nth-order standard normal PDF, $\mathbf{u}$ is the column vector of n standard normal variables, and $\mathbf{T}$ is the one-to-one mapping transformation matrix that satisfies $\mathbf{u} = \mathbf{T}(\mathbf{x})$. The evaluation of Eq. (3) can be difficult because a multidimensional integral is involved, the exact form of the joint PDF is rarely known, and the failure surface, $G(\mathbf{u}) = 0$, is not always provided in closed form. Within the context of the FORM, the probability of failure can be estimated by performing a linear approximation of the function $G(\mathbf{u})$ at the point $\mathbf{u}^*$. This point is characterized by a specific constrained optimization problem, as described subsequently:

$$\mathbf{u}^* = \min_{\mathbf{u}} f(\mathbf{u}) = \frac{1}{2}\mathbf{u}^{\mathrm{T}}\mathbf{u} \ \text{ subject to } \ G(\mathbf{u}) = 0 \tag{4}$$

where $\mathbf{u}^*$ is located on the limit-state surface satisfying $G(\mathbf{u}) = 0$, and its distance from the origin in the standard normal space is minimal. As an example of the first-order approximation concept of the FORM, the approximated LSF in the two-dimensional space is shown in Fig. 1. In the standard normal space, as shown in the figure, the equal probability density contours are concentric circles centered on the origin; therefore, $\mathbf{u}^*$, which is often called the most probable point (MPP) or the design point, has the highest probability among all points in the failure domain $G(\mathbf{u}) \le 0$. The first-order approximation of the failure probability is computed based on the probability content of the half-space in the standard normal space, defined by distance β, referred to as the reliability index. Therefore, P_f can be expressed in terms of the reliability index, as follows:

$$P_f = \Phi(-\beta) \tag{5}$$

where $\Phi(\cdot)$ denotes the standard normal cumulative distribution function.

One of the representative methods for solving the constrained optimization problem in Eq. (4) is the HLRF algorithm. Beginning from an initial point $\mathbf{u}_1 = \mathbf{T}(\mathbf{x}_1)$, a series of points is computed using a recursive formula, as follows:

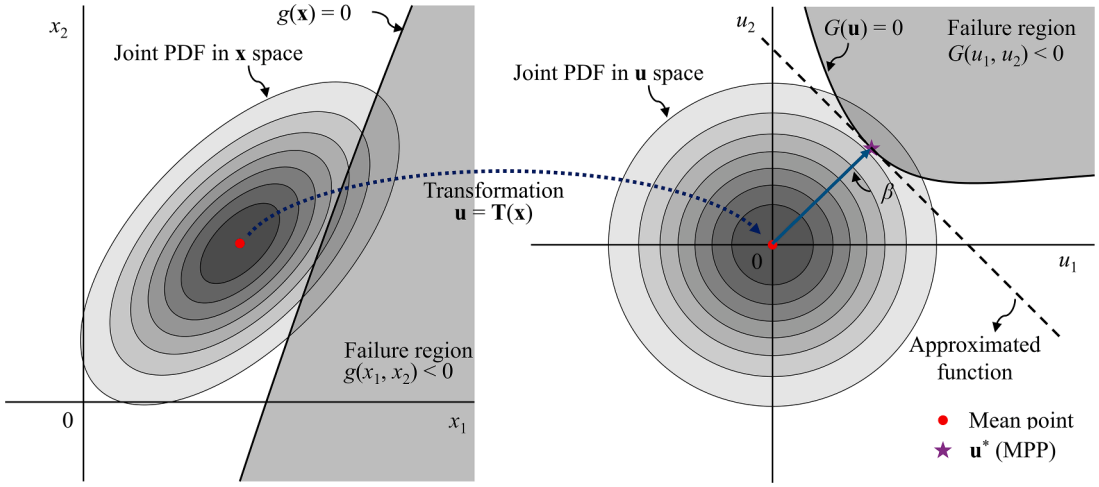

Fig. 1. Linear approximation in FORM.

$$\mathbf{u}_{i+1} = \mathbf{u}_i + \lambda_i \mathbf{d}_i \tag{6}$$

where $\mathbf{d}_i$ is the search direction vector at the i th iteration where $i = 1, 2, \ldots$, and λ_i is the step size. The search direction vector $\mathbf{d}_i$ designed for the objective function in Eq. (4) in the HLRF algorithm can be calculated as follows:

$$\mathbf{d}_i = \frac{1}{\| \nabla G(\mathbf{u}_i) \|^2} \left[\nabla G(\mathbf{u}_i)^{\mathrm{T}} \mathbf{u}_i - G(\mathbf{u}_i) \right] \nabla G(\mathbf{u}_i) - \mathbf{u}_i \tag{7}$$

where $\nabla G(\mathbf{u}) = [\partial G/\partial u_1, \ldots, \partial G/\partial u_{\mathrm{n}}]^{\mathrm{T}}$ denotes the gradient vector. In addition, various algorithms have been developed to determine the step size λ_i (Santos et al., 2012, Zhang & Der Kiureghian, 1995). In some cases where the limit-state function is non-convex or contains multiple minima, FORM analysis may not be suitable. Therefore, conducting a preliminary evaluation of the limit-state function can guide in selecting the appropriate reliability analysis method. More details regarding the FORM and its limitations are available in a paper by Der Kiureghian (Der Kiureghian, 2005).

2.2. HLRF–BFGS algorithm-based FORM

The HLRF algorithm is a classic algorithm that is widely used in the FORM. However, the lack of continuity of the gradient $\nabla G(\mathbf{u})$ for certain nonlinear problems in the FERA nullifies the fundamental assumption of the reliability formulation and may result in the non-convergence of the search algorithm (Haukaas & Der Kiureghian, 2006, Huang et al., 2019). Recently, Periçaro, Santos, Ribeiro, & Matioli (2015) proposed the BFGS algorithm (Fletcher, 2000), which is an iterative method for solving unconstrained nonlinear optimization problems to estimate the design point in the FORM. This algorithm, known as the HLRF–BFGS algorithm, can incorporate information regarding the curvature of the LSF, rendering it more robust and efficient than standard HLRF algorithms. In addition, the computation cost of the HLRF–BFGS algorithm is the same as that of the HLRF algorithm because it only requires one function and gradient evaluation for each iteration; hence, the number of LSF evaluations n_{FE} (i.e., the number of FE analyses) during FERA using the HLRF–BFGS-based FORM is

$$n_{FE} = (n_{RV} + 1) \times n_i \tag{8}$$

where n_{RV} and n_i denote the number of RVs and iterations, respectively.

The HLRF–BFGS algorithm calculates the search direction as follows:

$$\mathbf{d}_i = \frac{[\nabla G(\mathbf{u}_{i-1})^{\mathrm{T}} \mathbf{B}_{i-1} \mathbf{u}_{i-1} - G(\mathbf{u}_{i-1})] \mathbf{B}_{i-1} \nabla G(\mathbf{u}_{i-1})}{\nabla G(\mathbf{u}_{i-1})^{\mathrm{T}} \mathbf{B}_{i-1} \nabla G(\mathbf{u}_{i-1})} - \mathbf{B}_{i-1} \mathbf{u}_{i-1} \tag{9}$$

where $\mathbf{B}$ is the inverse of the Hessian matrix, which can be computed using the recursive BFGS updating formula as follows:

$$\mathbf{B}_i = \mathbf{B}_{i-1} + \left(1 + \frac{(\mathbf{q}_i)^{\mathrm{T}} \mathbf{B}_{i-1} \mathbf{q}_i}{(\mathbf{p}_i)^{\mathrm{T}} \mathbf{q}_i} \right) \frac{\mathbf{p}_i (\mathbf{p}_i)^{\mathrm{T}}}{(\mathbf{p}_i)^{\mathrm{T}} \mathbf{q}_i} - \frac{\mathbf{p}_i (\mathbf{q}_i)^{\mathrm{T}} \mathbf{B}_{i-1} + \mathbf{B}_{i-1} \mathbf{q}_i (\mathbf{p}_i)^{\mathrm{T}}}{(\mathbf{p}_i)^{\mathrm{T}} \mathbf{q}_i} \tag{10}$$

where

$$\mathbf{p}_i = \mathbf{d}_i \tag{11}$$

$$\mathbf{q}_i = \mathbf{d}_i + (\nabla G(\mathbf{u}_i) - \nabla G(\mathbf{u}_{i-1}))\xi_i \tag{12}$$

and ξ_i is the Lagrange multiplier expressed as

$$\xi_i = \frac{G(\mathbf{u}_{i-1}) - \nabla G(\mathbf{u}_{i-1})^{\mathrm{T}} \mathbf{B}_{i-1} \mathbf{u}_{i-1}}{\nabla G(\mathbf{u}_{i-1})^{\mathrm{T}} \mathbf{B}_{i-1} \nabla G(\mathbf{u}_{i-1})} \tag{13}$$

Hence, a new iteration point can be computed as follows:

$$\mathbf{u}_i = \mathbf{u}_{i-1} + \mathbf{d}_i \tag{14}$$

The algorithm is iterated until the following stopping criterion are satisfied:

$$1 - \frac{|\nabla G(\mathbf{u}_i)^{\mathrm{T}} \mathbf{u}_i|}{\| \nabla G(\mathbf{u}_i)^{\mathrm{T}} \| \cdot \| \mathbf{u}_i \|} \le \varepsilon_1 \quad \text{and} \quad |G(\mathbf{u}_i)| \le \varepsilon_2 \tag{15}$$

In the following numerical and application examples, ε_1, ε_2, and $i_{\max}$ are assumed to be 0.05, 0.05, and 30, respectively.

3. Computational platform integrated with FERUM and MIDAS/Civil

Two external software packages for reliability and structural analysis should be coupled to address the computational cost disadvantages of the MCS in FERA and to develop an efficient bridge safety assessment platform. FERUM is integrated with MIDAS/Civil, and an interface code is developed such that these two software packages can communicate with each other. The developed computational platform is termed FERUM–MIDAS. In this section, the developed structural reliability analysis platform, FERUM–MIDAS, is introduced in detail, and the verification of the numerical example analysis by the proposed platform is presented in the next section, by comparing the results with those of the HLRF–BFGS-based FORM and importance sampling (IS) (Melchers, 2018). By coupling reliability analysis software (i.e., FERUM) and structural analysis software (i.e., MIDAS/Civil), the proposed platform enables bridge safety assessment to be realized more efficiently at a lower computational cost.

3.1. Proposed platform: FERUM–MIDAS

FERUM, a reliability analysis package developed by researchers at the University of California at Berkeley, can perform a range of reliability analyses (Haukaas, 2003). FERUM offers functions for various reliability analysis methods, including the FORM, second-order reliability method (SORM), MCS, and importance sampling; furthermore, 16 types of probability distributions, including normal, lognormal, gamma, beta, and Gumbel distributions, are available in the package. In addition, the publicly accessible source code and its versatile features have led to FERUM's extensive application in diverse engineering problems. In this study, the source code of FERUM is partially modified to incorporate the HLRF-BFGS algorithm within the FORM framework.

MIDAS/Civil is a specialized commercial software package for civil engineering, with a focus on FE analysis of bridges. The software contains various structural analysis algorithms, such as dynamic, nonlinear, and construction phase analysis algorithms, as well as numerous analysis functions like moving load and hydration heat analysis. Moreover, it enables the structural analysis and design of diverse bridge structures, including pre-stressed concrete, cable-stayed, and suspension bridges.

In this study, a reliability-based safety assessment of a bridge structure is performed by constructing a platform using FERUM–MIDAS. Fig. 2 displays the approximate data flow of the proposed platform, which enables bidirectional communication between reliability analysis and structural analysis software. To solve the nonlinear constrained optimization problem in Eq. (4) using the FORM, $G(\mathbf{u}_i)$ and $\nabla G(\mathbf{u}_i)$ (i.e., the values and gradients of the LSF in the standard normal space, respectively) are required at each iteration step. However, if the LSF is not an analytical function of RVs, then gradient calculation during the FORM analysis can be challenging. To address this, an interface module between FERUM and MIDAS/Civil was developed so that FERUM can evaluate the LSF based on output responses (e.g., structural responses, such as force, stress, or displacement results from structural analysis using MIDAS/Civil), and the gradients are obtained numerically using the finite difference method, which is a widely-used numerical differentiation method includes forward, backward, and central difference approaches. The central difference method may offer higher accuracy than forward and backward difference methods; however, it requires additional structural analyses, leading to increased computational cost and thus should be considered carefully. Additionally, in the proposed platform, the reliability analysis package FERUM repeatedly calls MIDAS/Civil to obtain structural responses during the FORM analysis. During this process, the platform automates the reading and modification of input files for the FEA package in MIDAS/Civil, thereby streamlining iterative data flow and improving the overall efficiency of the analysis.

In contrast to other commercial structural analysis software packages such as ABAQUS® and ANSYS®, however, MIDAS/Civil cannot perform structural analysis in a disk operating system (DOS) environment; in other words, it can only perform structural analysis in a GUI environment. To address this issue, as shown in Fig. 2, a GUI control module using the Java Robot class (Ruiz & Price, 2007) embedded in MATLAB is newly developed and introduced into FERUM. The details of the GUI control module are shown in Fig. 3. Using the function of the robot class in FERUM–MIDAS, the GUI control module enables software operation and structural analysis, which cannot be realized in the DOS environment, via mouse and keyboard control commands, as shown in the figure. The proposed platform, FERUM–MIDAS, enables efficient structural reliability analysis owing to the GUI control module added in FERUM. In addition, repeated structural analyses can be performed by employing control modules from other FE analysis software packages that cannot be operated in DOS environments. While the proposed platform offers an efficient approach to reliability analysis through its GUI control module, an important consideration is that the physical use of the keyboard and mouse by the user may be temporarily restricted during the analysis process. This restriction arises from the characteristics of the GUI module, which automatically controls the software. If the user physically operates the keyboard or mouse during this process, the analysis may be interrupted or errors could occur. Therefore, it is crucial to avoid physical interference until all procedures are completed and the analysis is fully completed.

3.2. Implementation procedure of FERUM–MIDAS

To facilitate the understanding of the FORM using the HLRF–BFGS algorithm and to improve the usability of the proposed platform, its sequence is detailed below (see the flowchart in Fig. 4).

(1) Initialization: The step index $i = 0$ and convergence tolerances ε_1, ε_2, and $i_{\max}$ are specified. The starting point is $\mathbf{X}_0$, which is the

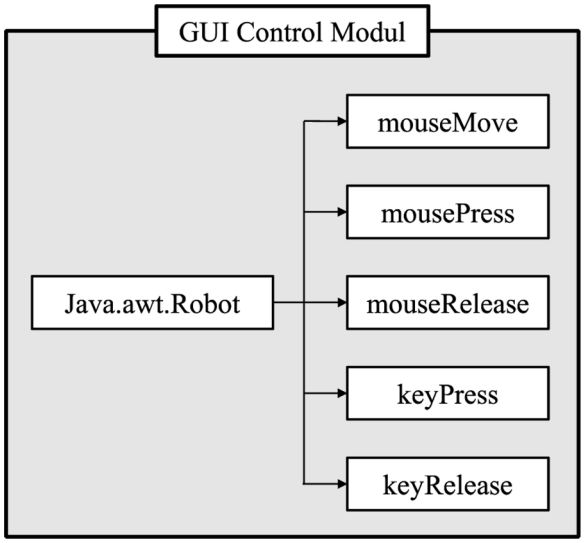

Fig. 3. Configuration of GUI control module.

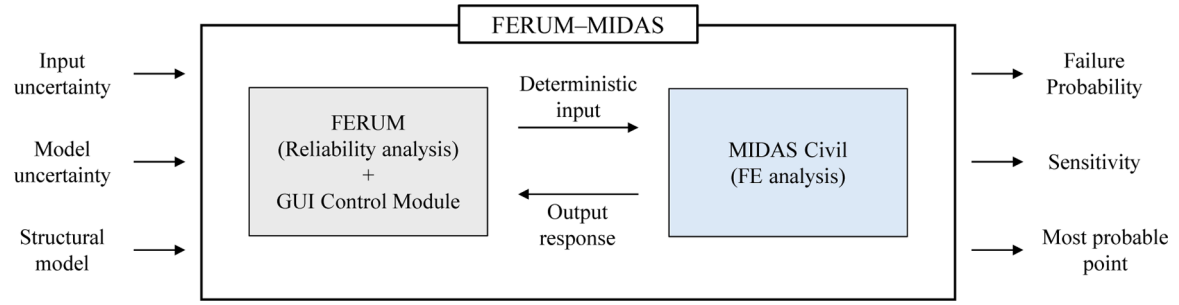

Fig. 2. Data flow of FERUM–MIDAS.

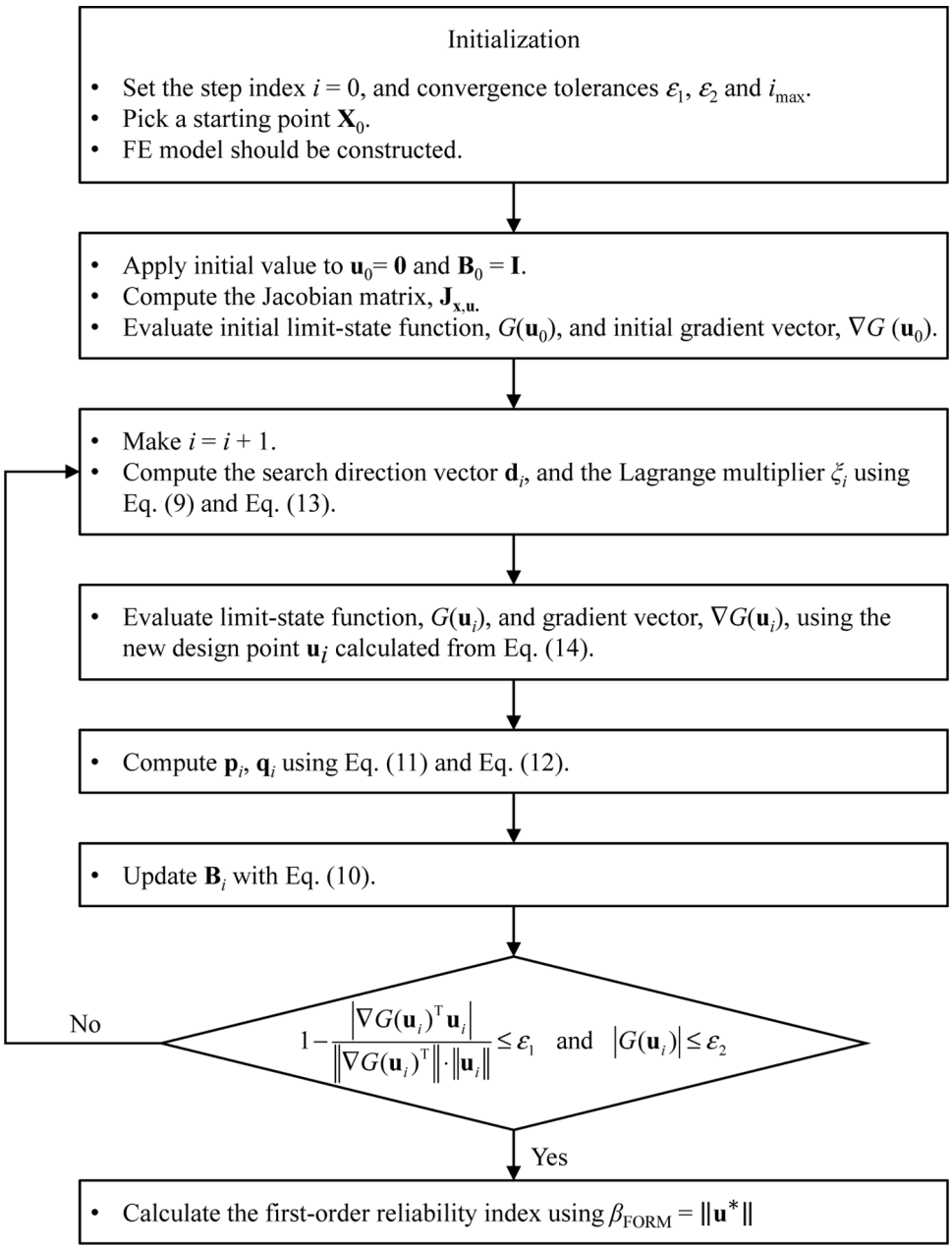

Fig. 4. Flowchart illustrating implementation procedure of FERUM–MIDAS.

mean vector for all RVs in **x**. In addition, an FE model for the FERA should be constructed.

(2) The initial value is applied to $\mathbf{u}_0 = \mathbf{0}$ and $\mathbf{B}_0 = \mathbf{I}$. The Jacobian matrix, $\mathbf{J}_{\mathbf{x},\mathbf{u}}$, which is the transformation from **x** to **u**, is computed. The initial LSF, $G(\mathbf{u}_0)$, and initial gradient vector, $\nabla G(\mathbf{u}_0)$, are evaluated based on the structural response (i.e., FE analysis results with the mean values of all RVs).

(3) A step index, $i = i + 1$, is considered. The search direction vector $\mathbf{d}_i$ and Lagrange multiplier ξ_i are computed using Eqs. (9) and (13), respectively:

(4) The LSF $G(\mathbf{u}_i)$ and gradient vector $\nabla G(\mathbf{u}_i)$ are evaluated using the new design point $\mathbf{u}_i$ calculated from Eq. (14).

(5) $\mathbf{p}_i$ and $\mathbf{q}_i$ are evaluated using Eqs. (11) and (12), respectively.

(6) The inverse of the Hessian matrix $\mathbf{B}_i$ is updated using Eq. (10).

Steps 3–6 are repeated until the stopping criterion in Eq. (15) are satisfied or the step index i reaches to i_{max}. Subsequently, the first-order reliability index, β, can be easily obtained as $\beta_{FORM} = \|\mathbf{u}^*\|$, where is the MPP. In addition, P_f can be computed using Eq. (5). As shown in Fig. 2, FERUM–MIDAS also provides sensitivity information for each RV. Therefore, users can quantitatively determine the importance of variables if necessary, without performing an additional sensitivity analysis.

4. Illustrative example for verification of FERUM–MIDAS computational platform

In several previous studies, comparisons were made between new reliability analysis methods and sampling-based methods such as crude Monte Carlo simulation and IS simulation (Lee & Moon, 2014, Haukaas, 2003, Lee et al., 2008, Kang et al., 2012, Moon et al., 2018, Lee et al., 2021, Lee et al., 2016, Kim et al., 2017, Lee et al., 2019, Der Kiureghian, 2005). Similarly, to verify the proposed platform and highlight its advantages, a numerical example is selected and solved, and the analysis results are compared with those from the IS method. For the sake of

simplicity, the target structure of the illustrative example is assumed to be a simply supported steel plate considering material nonlinearity, and its FE model is constructed for MIDAS/Civil. The structural analysis using the constructed FE model considers not only the self-weight, but also various vehicle loads, which provides the reliability index and failure probability when various types of vehicle loads including those exceeding weight limit.

4.1. MIDAS/Civil FE model of simply supported steel plate

The FE model constructed for MIDAS/Civil is shown in Fig. 5. The longitudinal length, transverse length, and thickness of the structure are 30.0, 5.0, and 0.2 m, respectively. The FE model is constructed by considering the steel material nonlinearity in EN 1993-1-5 (2006), as shown in Fig. 6. In the figure, f_y and ε_y denote the yield stress and yield strain of steel plate, respectively, and E represents the elastic modulus. E_{sh} represents the modulus of elasticity after the yielding (i.e., strain hardening) of steel and is assumed to be $E/100$. In addition, two types of loads are considered: the dead load (i.e., self–weight) and live load (i.e., vehicle load). Specifically, as the live load, the KL-510 load model (MOLIT, 2016), a design vehicle load model in Korea, is considered, and a crane vehicle model that exceeds the weight limit is employed.

4.2. Crane vehicle passage classification system exceeding weight limit

Recently, Yu et al. (2020) and Lee et al. (2020) proposed a Korean classification system for the passage of permitted crane vehicles that exceeded the limit weight and used it for the safety assessment of bridges. The permitted vehicles (Lee et al., 2020) were hydraulic crane vehicles that weighed 12 tons (i.e., 117.7 kN), including 2-to 9-axle cranes. The classification of licensed vehicles comprises three licensing schemes: Routine Permit, Special Permit 1, and Special Permit 2, as shown in Table 1. Routine Permit and Special Permit 1 allow the simultaneous passage of general vehicles; however, Special Permit 2 stipulates a vehicle with a total weight exceeding 80 tons, which is more than twice the weight of the restricted vehicle, such that it can be driven alone. The KL-510 lane load model was loaded considering the series effect of permitted vehicles, and the weight of permitted vehicles was reduced by 0.8 times to obtain the equivalent load effect as the actual traffic situation. In this study, safety assessments are performed on Special Permit 1 and Special Permit 2 considering the characteristics of the series and parallel effects described in Yu et al. (2020) and Lee et al. (2020).

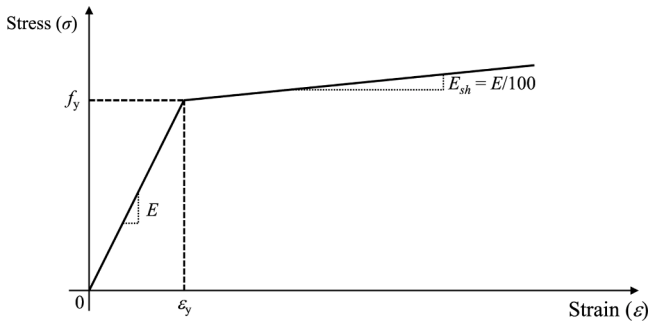

Fig. 6. Stress–strain curve of steel material (EN 1993-1-5, 2006).

Table 1
Classification of permit type, regulations, and crane axle.

Permit type	Regulations			Crane axle
	Period	Frequency	Loading condition	
Routine Permit	<1 year	Unlimited passage	Mix with normal traffic	Two, three, and four axle cranes
Special Permit 1	30–90 days	<100 passages	Mix with normal traffic	Five and six axle cranes
Special Permit 2	–	Single passage only	Permitted vehicle only	Seven, eight, and nine axle cranes

4.3. Input vehicle load model

The vehicle loads used in this study are the designed vehicle live load in the Korea Highway Bridge Design Code (KHBDC)-Limit State Design (LSD) (MOLIT, 2016) and the hydraulic crane with Special Permit 1 and

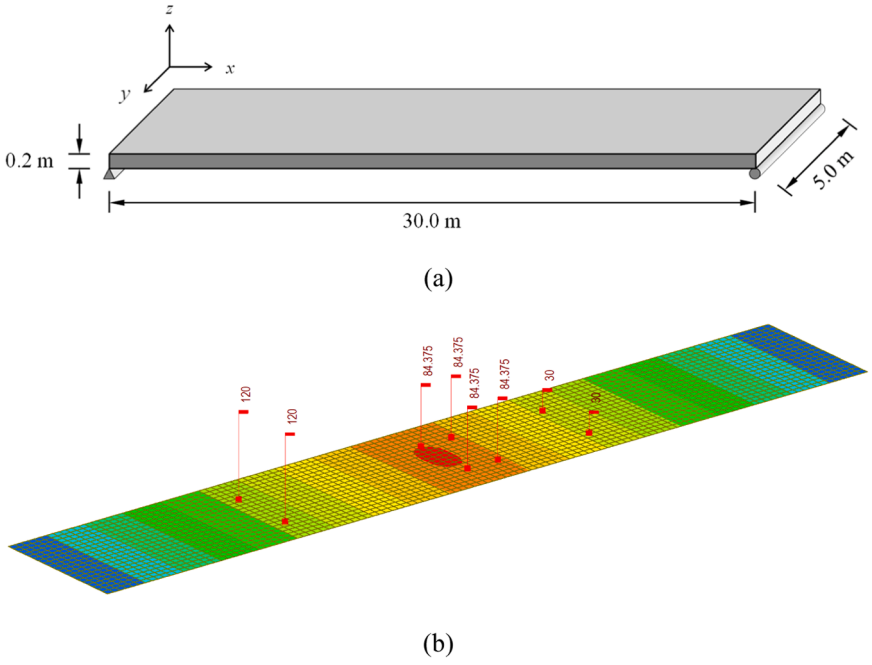

Fig. 5. MIDAS/Civil FE model: (a) Geometry of simply supported steel plate structure, (b) Example of FE analysis of KL-510 vehicle model constructed using MIDAS/Civil.

Special Permit 2 (i.e., 5- to 9-axle cranes). The axle weight and specifications of the designed vehicle load model KL-510 are shown in Fig. 7. In KHBDC-LSD, the design vehicle load selects the more prominent load effect among the standard truck loads or 75 % of the standard truck loads with a 12.7 kN/m standard lane load. The standard lane load is evenly distributed in the longitudinal direction and is applied differently to the span; if the span length exceeds 60 m, then the standard lane load is calculated as $12.7 \times \left(\frac{60}{L}\right)^{0.10}$, which is reduced based on the span length L. Additionally, it is evenly distributed in the horizontal direction with a width of 3.0 m, and the impact factor is not applied to the standard lane load. The axle weight and specifications of the hydraulic cranes with Special Permit 1 and Special Permit 2 employed in this study are listed in Table 2. The loading methods of the permitted vehicles, considering the series effects, are summarized in Table 3.

4.4. Analysis results

In this verification example, five types of uncertainties are considered and assumed as RVs: the ultimate strength of steel, yield strength of steel, elastic modulus (i.e., Young's modulus), dead load, and live load. The first, second, and third uncertainties are those of material properties or supply, whereas the fourth and fifth uncertainties are those of the load or demand. In addition, for the sake of simplicity, it is assumed that the RVs are statistically independent of each other. The statistical properties (i.e., the mean, coefficient of variation, and probability distribution type) of the RVs are summarized in Table 4. In addition, in the limit-state of the structure considered in this example, the failure probability is calculated as the event in which the stress of the structure exceeded the limit strength of the steel material. Therefore, the LSF, $g(\mathbf{x})$, is defined as follows:

$$g(\mathbf{x}) = f_u(\mathbf{x}) - f(\mathbf{x}) \leq 0 \tag{16}$$

where f_u is the ultimate steel strength and f is the maximum von Mises stress from the FE analysis results.

To verify the proposed platform, the reliability index (β) is computed first using two methods: the FORM based on the HLRF–BFGS algorithm using FERUM–MIDAS, and the importance sampling method. The importance sampling method is known to be more efficient than the crude MCS (Melchers, 2018), and it enables the significant reduction of the number of samples (i.e., FE analyses) required to get converged results. In this study, the coefficient of variation of the results from importance sampling is estimated based on a previous study (Givens & Hoeting, 2012), and the threshold value is set to be 0.05. Further details regarding the importance sampling method are available in Melchers (Melchers, 2018).

The probability of structural failure for a limit-state is calculated using the FERUM–MIDAS structural reliability analysis platform, and the results are compared with those obtained using the importance sampling method, as shown in Table 5 and Fig. 8. To check the computational efficiency, the number of structural analyses required to calculate the same probability level of failure for each KL-510 load model and permitted vehicle (i.e., 5- to 9-axle cranes) load models are compared for each method. Table 5 shows that the proposed method can provide the similar failure probability with importance sampling even though it requires a smaller number of structural analyses. In addition, Fig. 8 shows that the reliability index from importance sampling for each of the six vehicle load models converges as the number of samples (i.e., FE simulations) increases. On the other hand, the proposed method exhibits a stepwise reliability index due to the batch update process for gradient estimation, as outlined in Eq. (8). For example, with five RVs, each iteration requires six structural analyses—one for evaluating the limit-state function and five for calculating gradients for each RVs—resulting in a stepwise pattern in the index value.

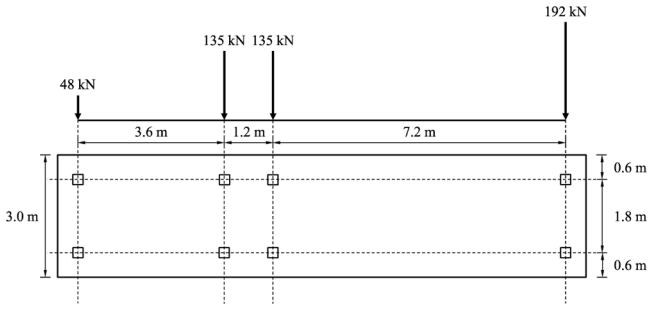

Fig. 7. KL–510 standard truck model of KHBDC-LSD (MOLIT, 2016).

5. Application to in-service bridge

In this Section, the proposed platform, FERUM-MIDAS, is applied to a more complicated and realistic example, which is an in-service bridge in the Republic of Korea. For security reasons, the target bridge is called the A-bridge in this study. Based on the structural design drawing of the target bridge, an FE model is constructed for MIDAS/Civil, and a reliability-based safety assessment considering the uncertainty of material properties and various load types is performed using FERUM-MIDAS.

5.1. Description of in-service A-bridge

The A-bridge, shown in Fig. 9, is a bridge with a total length of 1913.00 m, and the upper structure of this bridge comprises a continuous three-span steel orthotropic plate- type deck box girder. The steel deck box girder of this bridge, which is subject to safety assessment, has a main span of 80.00 m and a width of 14.30 m on the top and bottom; furthermore, it comprises two rows of girders with a height of 3.50 m, horizontal ribs, vertical ribs, and bracing. The bridge was designed in compliance with the Korea Standard Specification for Highway Bridges (MOC, 1983), and its construction was completed in 1984. The dimensions and shape of the longitudinal section and the typical cross-section of the A-bridge are shown in Fig. 10.

As shown in Fig. 11, the MIDAS/Civil FE model of the bridge is established based on its original structural design and management history information. In this application example, the segment where the FE model is constructed is one to three spans (i.e., 3×80 m $= 240$ m), which is 1/4 of the main bridge (960 m) of the A-bridge. In addition, the FE model is constructed in three dimensions using the main girder and horizontal rib, the vertical rib as plate elements, and bracing as frame elements. The steel material used as the main member of the steel deck plate, web, lower flange, vertical rib, transverse rib, and diaphragm is SM520B, and the auxiliary member used for vertical and horizontal reinforcement is SM400B. In addition, the stress–strain curve of the steel member shown in Fig. 6 is introduced to account for the material nonlinearities.

Self-weight, railing, curb, and other loads are considered as dead loads exerting on the bridge, whereas live loads are analyzed considering the KL-510 load and permitted vehicle models. In this application example, a Korean classification system for the permitted vehicle loading method proposed by Yu et al. (2020) and Lee et al. (2020) introduced in the previous section is applied, and the results are summarized in Tables 1, 2, and 3. Furthermore, because the A-bridge is a three-lane bridge, the multilane loading system proposed in Lee et al. (2020) is applied, and multilane presence factors considering the parallel effect for permitted vehicles are described in Table 6.

5.2. Reliability-based bridge safety assessment result

In this application example, eight uncertainties are regarded as RVs: the steel ultimate strength (f_u), steel yield strength (f_y), elastic modulus

Table 2
Axle weight and specifications of hydraulic crane vehicle.

Permit type	Axle distance and weight	wheel width (m)
Special Permit 1	5-axle 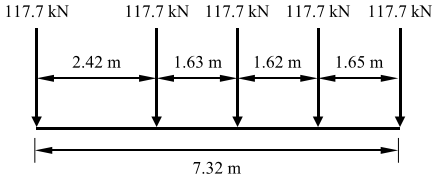	2.350
	6-axle 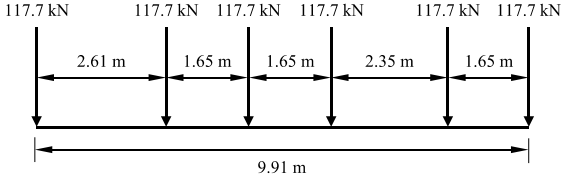	2.585
Special Permit 2	7-axle 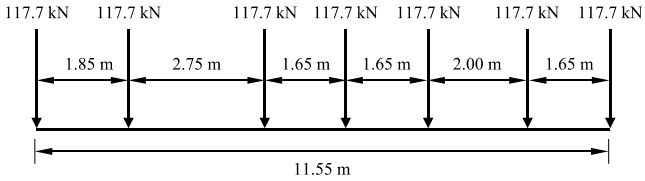	2.612
	8-axle 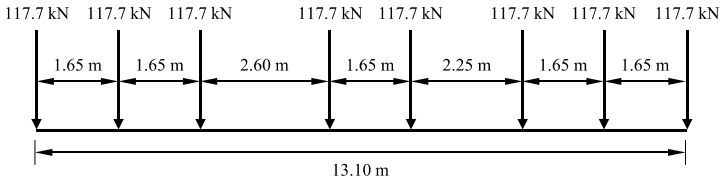	2.612
	9-axle 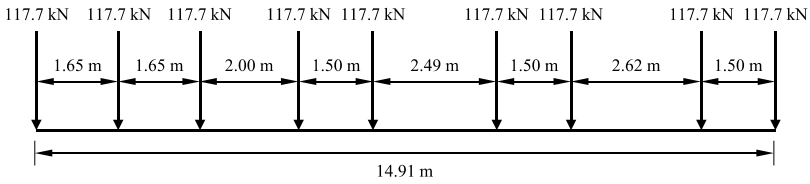	2.563

Table 3
Loading procedure considering series effect for permitted vehicles.

Permit type	Loading method and impact factor
Special Permit 1	(i) Single loading of permitted vehicle (ii) 80 % of permitted vehicles + standard lane load - Compare (i) and (ii) and select the more prominent load effect - Apply an impact factor of 0.25 to vehicle load
Special Permit 2	- Single loading of permitted vehicles - Impact factor: 0.20

Table 4
Statistical properties of RVs for steel plate example.

Random variables (RVs)	Mean	Coefficient of variation	Distribution type
Steel ultimate strength (f_u)	410 [MPa]	0.05	Normal
Steel yield strength (f_y)	235 [MPa]	0.08	Log-normal
Steel elastic modulus (E)	205 [GPa]	0.06	Normal
Dead load (DL)	1	0.10	Normal
Live load (LL)	1	0.20	Log-normal

(E), self-weight of steel members (D_1), self-weight of cast-in-place concrete (D_2), pavement load (D_3), KL-510 load model (L_1), and permitted vehicle model (L_2). The RVs are assumed to be statistically independent of each other, and their statistical characteristics were determined based on previous studies (Lee, 2014, Nowak, 1999, VanDerHorn & Wang, 2011), as summarized in Table 7. Additionally, the statistical characteristics of the crane are assumed to be the same as those of the KL-510 load model. In this study, the LSF is defined by Eq. (16), and the structural response is derived from the results of the nonlinear FE analysis.

Using the proposed FERUM-MIDAS, the probability of structural failure for a limit-state is calculated, and the reliability index is obtained to evaluate the safety of the A-bridge. The results for each vehicle load model are presented in Table 8. Using the proposed platform, the reliability index for each vehicle load model is successfully calculated via a few MIDAS/Civil non-linear FE analyses, and the safety of the A-bridge is evaluated efficiently.

In the case of Special Permit 1 (i.e., 5- and 6-axle cranes), the total weight applied to the bridge is similar or slightly larger than that of the KL-510 vehicle. Hence, the reliability index obtained from the proposed platform is almost similar to or slightly lower than that of the KL-510 vehicle load model. However, Special Permit 2 (i.e., 7- to 9-axle cranes) is not affected by the lane load because it involves single loading without the series effect. Therefore, in the case of an A-bridge with a long span, the effect of the lane load can be considered dominant, and the reliability index calculated is relatively higher than those of the KL-510 load model and Special Permit 1. In addition, the reliability index decreases as the total weight of the crane load model increased from 7- to 9-axle crane.

Table 5
Comparison of probability of failure and reliability index obtained by two methods.

Vehicle load model	Reliability index, β		Failure probability, P_f		Number of structural analyses	
	Proposed method	IS simulation	Proposed method	IS simulation	Proposed method	IS simulation
KL-510	1.638	1.638	5.07×10^{-2}	5.07×10^{-2}	18	809
5-axle	2.058	2.078	1.98×10^{-2}	1.89×10^{-2}	18	1020
6-axle	1.675	1.716	4.70×10^{-2}	4.31×10^{-2}	18	871
7-axle	1.633	1.632	5.12×10^{-2}	5.13×10^{-2}	24	804
8-axle	1.263	1.264	1.03×10^{-1}	1.03×10^{-1}	18	693
9-axle	0.956	0.955	1.70×10^{-1}	1.70×10^{-1}	36	580

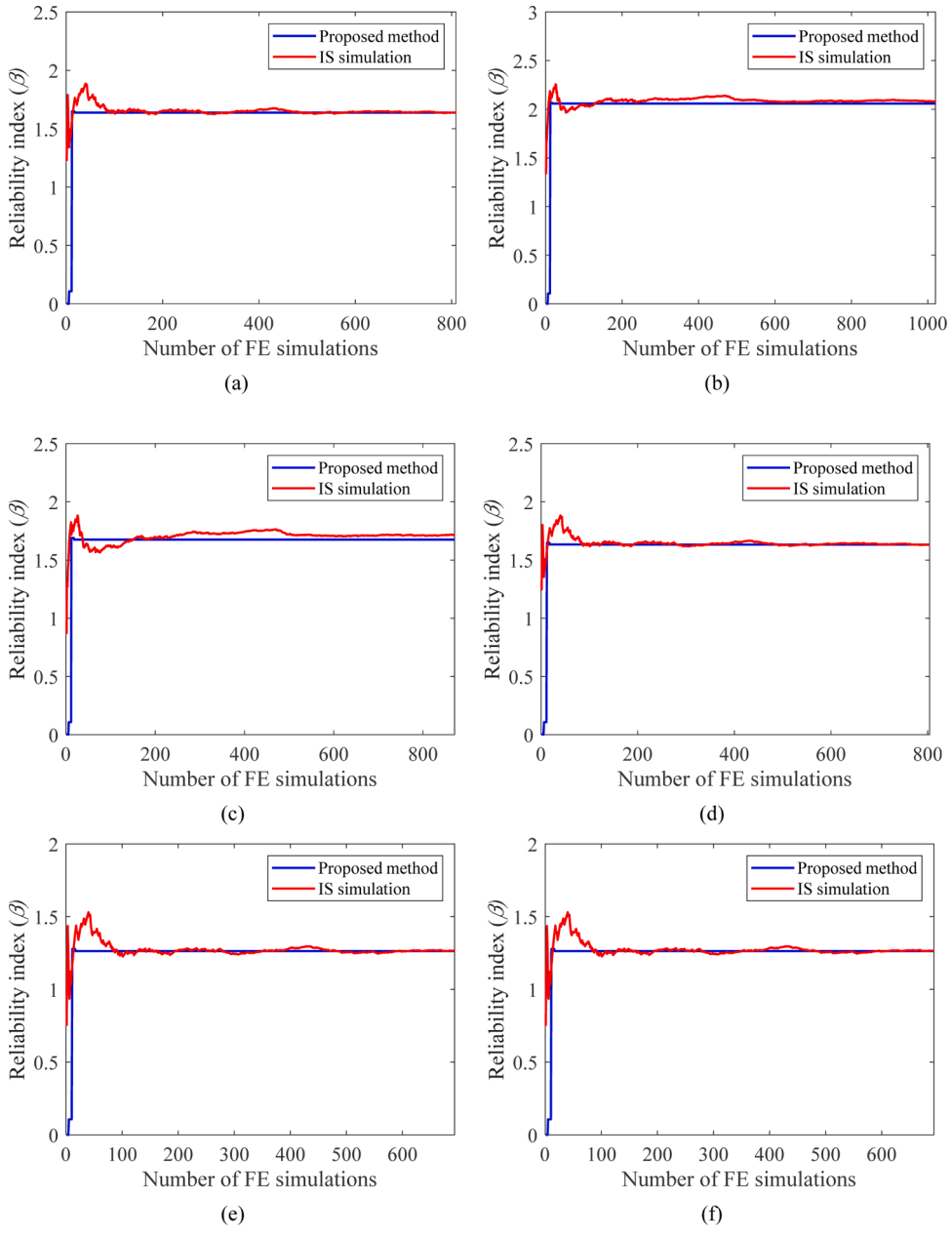

Fig. 8. Comparison of the reliability index obtained from IS simulation with the number of FE simulations for six vehicle load models and FERUM-MIDAS results: (a) KL-510 model, (b) 5-axle crane, (c) 6-axle crane, (d) 7-axle crane, (e) 8-axle crane, and (f) 9-axle crane.

The American Association of State Highway and Transportation Officials (AASHTO) Bridge Design Code (AASHTO LRFD, 2017) recommends a target reliability index of 3.5 (i.e., a failure probability of 2.326×10^{-4}) with a service life of 75 years for steel and prestressed concrete components. Using the KL-510 vehicle load model and the crane load model that applies the permitted vehicle loading system proposed by Yu et al. (2020) and Lee et al. (2020), it is observed that the A-bridge satisfies the target reliability index proposed by the AASHTO Bridge Design

Fig. 9. Photograph of A-bridge.

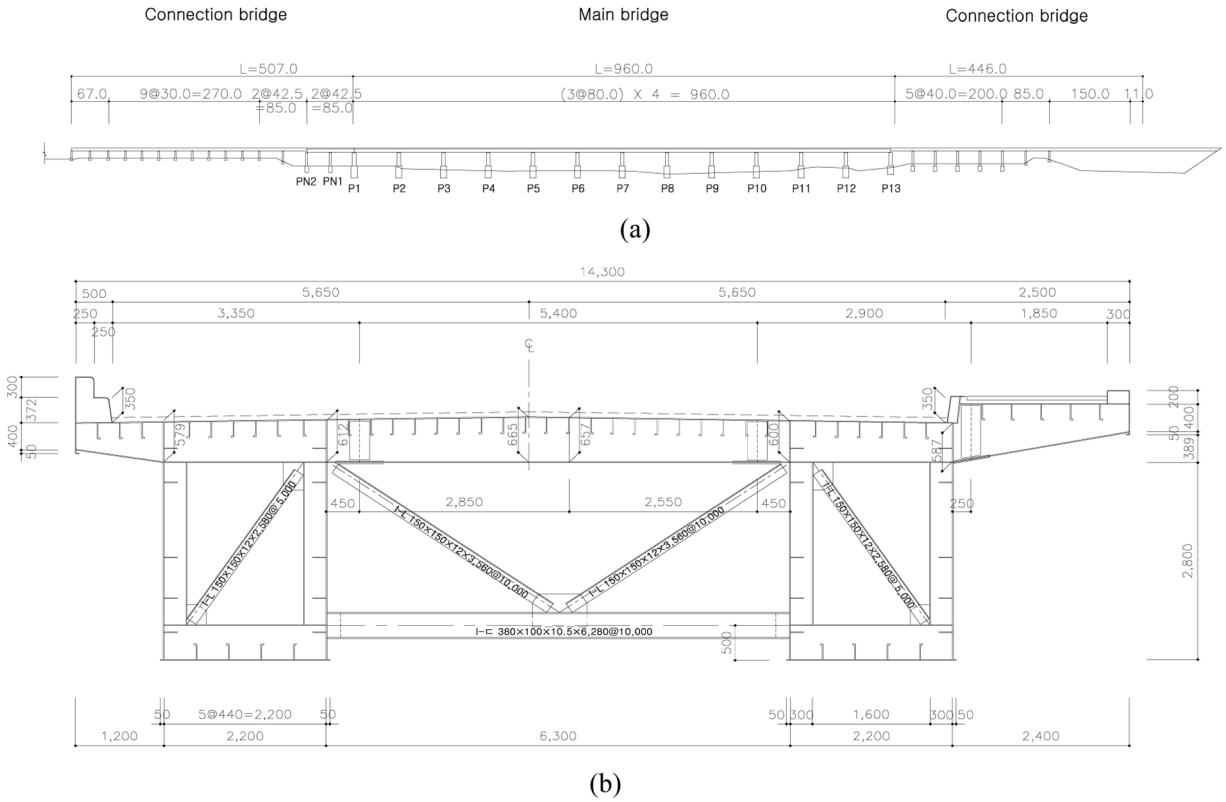

Fig. 10. Schematic cross section of A-bridge: (a) Longitudinal section of bridge, (b) Typical cross section of main bridge.

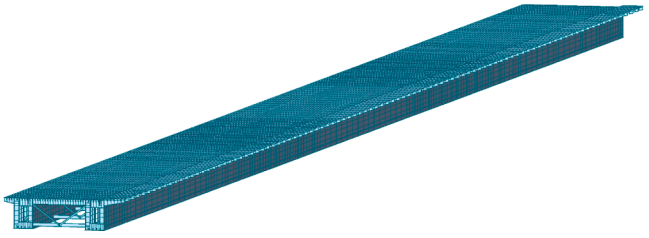

Fig. 11. FE model of A-bridge constructed using MIDAS/Civil.

Code. Therefore, it is predicted that the A-bridge can sufficiently secure safety for the KL-510 vehicle load model and crane load model.

6. Conclusion

A new computational platform, FERUM-MIDAS is proposed for evaluating the reliability-based structural safety of bridges. The computational platform integrates sophisticated software packages, FERUM and MIDAS/Civil, for reliability and structural analyses at a

Table 6
Loading procedure and multilane presence factors considering parallel effect for permitted vehicles.

Permit type	Loading method and multilane presence factors
Special Permit 1	- Permitted vehicles are loaded only in the outermost lane; multilane load factor is not applied - Design vehicle load model and multilane presence factor are applied to other lanes (i) Multi-lane presence factor for loading one lane: 0.9 (ii) Multi-lane presence factor for loading two lanes: 0.8 (iii) Multi-lane presence factor for loading three lanes: 0.7 (iv) Multi-lane presence factor for loading more than four lanes: 0.65
Special Permit 2	- Single loading of permitted vehicles

Table 7
Statistical properties of RVs for bridge example.

Random variables (RVs)	Nominal values	Bias factor	Coefficient of variation	Distribution type
Steel ultimate strength (f_u)	520.00 [MPa]	1.05	0.05	Normal
Steel yield strength (f_y)	355.00 [MPa]	1.10	0.08	Log-normal
Elastic modulus (E)	205.94 [GPa]	1.00	0.06	Normal
Self-weight of steel members (D_1)	1.00	1.03	0.08	Normal
Self-weight of cast-in-place concrete (D_2)	1.00	1.05	0.10	Normal
Pavement load (D_3)	1.00	1.00	0.25	Normal
KL-510 load model (L_1)	1.00	1.00	0.20	Log-normal
Permitted vehicle model (L_2)	1.00	1.00	0.20	Log-normal

Table 8
Reliability index and failure probability for the example bridge calculated using FERUM–MIDAS.

Vehicle load model	Reliability index, β	Failure probability, P_f
KL-510	5.003	2.822×10^{-7}
5-axle	4.998	2.896×10^{-7}
6-axle	4.913	4.485×10^{-7}
7-axle	5.657	7.702×10^{-9}
8-axle	5.518	1.714×10^{-8}
9-axle	5.377	3.787×10^{-8}

lower computational cost compared with simulation-based methods. In addition, a GUI control module is implemented in FERUM to control the GUI of MIDAS/Civil and perform a smooth structural reliability analysis. Because the proposed method performs reliability analysis using the FORM based on the recently developed HLRF–BFGS algorithm, it is expected to be more advantageous in terms of convergence, even when the nonlinearity of the LSF is significant.

The proposed platform is applied to a numerical example of a simply supported steel plate first. The results obtained from FERUM-MIDAS are compared with those from importance sampling, and it is observed that the proposed platform can provide accurate reliability index and failure probability results efficiently. In addition, a reliability-based safety assessment is performed using the proposed platform on an actual in-service bridge (i.e., A-bridge) in Korea. In the application example, the KL-510 vehicle load model and an overweight crane load model are evaluated, with results showing that the A-bridge meets the target reliability index recommended by ASSHTO for six vehicle loading scenarios. These outcomes indicate that FERUM-MIDAS provides a practical and reliable solution for efficient bridge safety assessments.

Additionally, FERUM-MIDAS has potential applications in evaluating the structural behavior of existing bridges under various loading conditions, such as wind, seismic, and live loads. By integrating FERUM and MIDAS/Civil, comprehensive analyses of bridge responses can be performed, enabling systematic evaluations of structural integrity and safety. Furthermore, the nonlinear, time history, and pushover analysis features of MIDAS/Civil allow for reliability analyses based on detailed structural modeling, which can be applied to various bridge types, including prestressed concrete, composite, and cable-stayed bridges. While these capabilities provide a robust framework for reliability-based safety evaluations of bridge structures, realizing such extensions requires further research and validation to expand the platform's applicability and enable more precise safety assessment.

CRediT authorship contribution statement

Seungjun Lee: Writing – review & editing, Writing – original draft, Visualization, Validation, Software, Methodology, Investigation, Formal analysis, Data curation, Conceptualization. **Young-Joo Lee:** Writing – review & editing, Writing – original draft, Supervision, Project administration, Methodology, Funding acquisition, Formal analysis, Conceptualization.

Declaration of competing interest

The authors declare that they have no known competing financial interests or personal relationships that could have appeared to influence the work reported in this paper.

Acknowledgements

This work was supported by the National Research Foundation of Korea (NRF) grant funded by the Korea government (MSIT) (No. RS-2024-00352879). This work was also supported by the Korea Agency for Infrastructure Technology Advancement (KAIA) grant funded by the Ministry of Land, Infrastructure and Transport (Grant RS-2021-KA163162).

References

AASHTO LRFD. (2017). *Bridge design specifications*. Washington, DC: American Association of State Highway and Transportation Officials (AASHTO).

Cao, H., Zhou, Y. L., Chen, Z., & Wahab, M. Abdel (2017). Form-finding analysis of suspension bridges using an explicit iterative approach. *Structural Engineering and Mechanics, 62*, 85–95. https://doi.org/10.12989/sem.2017.62.1.085

Cook, W., Barr, P. J., & Halling, M. W. (2015). Bridge failure rate. *Journal of Performance of Constructed Facilities, 29*, Article 04014080. https://doi.org/10.1061/(ASCE)CF.1943-5509.0000571

Crespi, P., Zucca, M., Valente, M., & Longarini, N. (2022). Influence of corrosion effects on the seismic capacity of existing RC bridges. *Engineering Failure Analysis, 140*, Article 106546. https://doi.org/10.1016/j.engfailanal.2022.106546

Der Kiureghian, A. (2005). *First- and second-order reliability methods, engineering design reliability handbook*. Boca Raton: FL:CRC Press. Chap. 14.

Der Kiureghian, A., & Taylor, R. L. (1983). In *Numerical methods in structural reliability. Proceedings of the Fourth International Conference on Applications of Statistics and Probability in Civil Engineering (ICASP4)*. Florence, Italy.

EN 1993-1-5. (2006). *Eurocode 3: Design of steel structures - Part 1-5: Plated structure elements*. European Committee for Standardization (CEN).
Estes, A. C., & Frangopol, D. M. (1999). Repair optimization of highway bridges using system reliability approach. *Journal of Structural Engineering, 125*, 766–775. https://doi.org/10.1061/(ASCE)0733-9445(1999)125:7(766)
Fletcher, R. (2000). *Newton-Like methods, practical methods of optimization*. New York: John Wiley & Sons. Chap. 3.
Fu, G. (2013). *Bridge design and evaluation: LRFD and LRFR*. New York: John Wiley & Sons.
Givens, G. H., & Hoeting, J. A. (2012). *Simulation and Monte Carlo integration*. New York: Computational Statistics, O'Reilly Media. Chap.6.
Gollwitzer, S., Kirchgaßner, B., Fischer, R., & Rackwitz, R. (2006). PERMAS-RA/STRUREL system of programs for probabilistic reliability analysis. *Structural Safety, 28*, 108–129. https://doi.org/10.1016/j.strusafe.2005.03.008
Haldar, A. (2006). *Recent developments in reliability-based civil engineering*. Singapore: World Scientific Publishing Company.
Haukaas, T. (2003). *Finite element reliability and sensitivity methods for performance-based engineering, ph.d. dissertation*. Berkeley, CA, USA: University of California.
Haukaas, T., & Der Kiureghian, A. (2006). Strategies for finding the design point in non-linear finite element reliability analysis. *Probabilistic Engineering Mechanics, 21*, 133–147. https://doi.org/10.1016/j.probengmech.2005.07.005
Ho, H., & Nishio, M. (2020). Evaluation of dynamic responses of bridges considering traffic flow and surface roughness. *Engineering Structures, 225*, Article 111256. https://doi.org/10.1016/j.engstruct.2020.111256
Huang, P., Huang, H. Z., & Huang, T. (2019). A novel algorithm for structural reliability analysis based on finite step length and Armijo line search. *Applied Sciences, 9*, 2546. https://doi.org/10.3390/app9122546
Huang, X., Hou, S., Liao, M., & Zhu, Z. (2018). Bearing capacity evaluation and reinforcement analysis of bridge piles under strong earthquake conditions. *KSCE Journal of Civil Engineering, 22*, 1295–1303. https://doi.org/10.1007/s12205-017-1352-9
Hwang, E.-S., & Kim, D.-Y. (2019). Live load model for long span steel cable bridges considering traffic congestion scenarios. *International Journal of Steel Structures, 19*, 1996–2009. https://doi.org/10.1007/s13296-019-00259-7
Hwang, E.-S., Nguyen, T. H., & Kim, D.-Y. (2013). Live load factors for reliability-based bridge evaluation. *KSCE Journal of Civil Engineering., 17*, 499–508. https://doi.org/10.1007/s12205-013-0561-0
Imam, B. M., & Chryssanthopoulos, M. K. (2012). Causes and consequences of metallic bridge failures. *Structural Engineering International, 22*, 93–98. https://doi.org/10.2749/101686612x13216060213437
Kang, W.-H., Lee, Y.-J., Song, J., & Gencturk, B. (2012). Further development of matrix-based system reliability method and applications to structural systems. *Structure and Infrastructure Engineering, 8*, 441–457. https://doi.org/10.1080/15732479.2010.539060
Kim, H., Sim, S.-H., Lee, J., Lee, Y.-J., & Kim, J.-M. (2017). Flood fragility analysis for bridges with multiple failure modes. *Advances in Mechanical Engineering, 9*, Article 1687814017696415. https://doi.org/10.1177/1687814017696415
Lee, J., Lee, Y.-J., Kim, H., Sim, S.-H., & Kim, J.-M. (2016). A new methodology development for flood fragility curve derivation considering structural deterioration for bridges. *Smart Structures and Systems, 17*, 149–165. https://doi.org/10.12989/sss.2016.17.1.149
Lee, J., Lee, Y.-J., Sim, S.-H., & Cho, S. (2019). A new probabilistic framework for structural system fragility and sensitivity analysis of concrete gravity dams. *KSCE Journal of Civil Engineering, 23*, 3592–3605. https://doi.org/10.1007/s12205-019-2282-5
Lee, S., Moon, D.-S., Kim, B., Kim, J., & Lee, Y.-J. (2021). Hybrid fragility curve derivation of buildings based on post-earthquake reconnaissance data. *Smart Structures and Systems, 28*, 553–566. https://doi.org/10.12989/sss.2021.28.4.553
Lee, S. H. (2014). *Calibration of the load-resistance factors for the reliability-based design of cable-supported bridges, ph.d. dissertation*. Seoul, Korea: Seoul National University.
Lee, S.-J., Yu, S. S., Park, Y., & Paik, I. (2020). Safety evaluation of concrete bridges for passage of crane vehicle exceeding weight limit. *Korea Institute for Structural Maintenance and Inspection, 24*, 92–101. https://doi.org/10.11112/JKSMI.2020.24.6.92 (in Korean).
Lee, Y.-J., & Moon, D.-S. (2014). A new methodology of the development of seismic fragility curves. *Smart Structures and Systems, 14*, 847–867. https://doi.org/10.12989/sss.2014.14.5.847
Lee, Y.-J., Song, J., & Tuegel, E. J. (2008). Finite element system reliability analysis of a wing torque box. *Proceedings of the 10th AIAA Nondeterministic Approaches Conference*. https://doi.org/10.2514/6.2008-1718. Schaumburg, IL.
Li, Y., Zhao, J., Bao, L., Dong, L., & Wang, Q. (2021). Numerical and theoretical analysis of spatial shear lag effect in through wide box bowstring arch bridge main girder. *Structures, 33*, 141–151. https://doi.org/10.1016/j.istruc.2021.04.049
Lin, S. W., Yi, T. H., Li, H. N., & Ren, L. (2017). Damage detection in the cable structures of a bridge using the virtual distortion method. *Journal of Bridge Engineering, 22*, Article 04017039. https://doi.org/10.1061/(ASCE)BE.1943-5592.0001072
Liu, P. L., Lin, H. Z., & Der Kiureghian, A. (1989). *CalREL user manual. report no. UCB/SEMM-89/18*. Berkeley, CA, USA: University of California.
Liu, Y., Zhou, J., Su, J., & Zhang, J. (2023). Residual capacity assessment of in-service concrete box-girder bridges considering traffic growth and structural deterioration. *Structural Engineering and Mechanics, 85*, 531. https://doi.org/10.12989/sem.2023.85.4.531
Lu, P., Zhuang, Y., Nabizadeh, A., & Tabatabai, H. (2020). Analytical and experimental evaluation of repairs to continuous PC girder bridge. *Journal of Performance of Constructed Facilities, 34*, Article 04019086. https://doi.org/10.1061/(ASCE)CF.1943-5509.0001358
Melchers, R. E. (2018). *Structural reliability: Analysis and prediction, third ed*. New York, NY, USA: John Wiley & Sons.
Meng, X., & Zhang, C. (2014). Extradosed and intradosed cable-stayed bridges with continuous cables: Conceptual consideration. *Journal of Bridge Engineering, 19*, 5–14. https://doi.org/10.1061/(ASCE)BE.1943-5592.0000477
MIDAS/Civil 2020 (ver 3.1), Midas/It, 2020. https://www.midasbridge.com/en/main (accessed 1 Jun. 2024).
MOC. (1983). *Korea Standard Specification for Highway Bridges*. Korea: Ministry of Construction (MOC).
MOLIT. (2016). Korea Highway Bridge Design Code (Limit State Design). *Ministry of Land, Infrastructure and Transport (MOLIT)*. Korea.
Moon, D. S., Lee, Y.-J., & Lee, S. (2018). Fragility analysis of space reinforced concrete frame structures with structural irregularity in plan. *Journal of Structural Engineering, 144*, Article 04018096. https://doi.org/10.1061/(ASCE)ST.1943-541X.0002092
Nowak, A. S. (1999). *Calibration of lrfd bridge design code, nchrp report 368*. Washington, DC: Transportation Research Board.
Nowak, A. S., & Szerszen, M. M. (2000). Structural reliability as applied to highway bridges. *Progress in Structural Engineering and Materials, 2*, 218–224. https://doi.org/10.1002/1528-2716(200004/06)2:2<218::AID-PSE27>3.0.CO;2-8
Park, K.-J., Kim, D.-Y., & Hwang, E.-S. (2018). Investigation of live load deflection limit for steel cable stayed and suspension bridges. *International Journal of Steel Structures, 18*, 1252–1264. https://doi.org/10.1007/s13296-018-0108-9
Periçaro, G. A., Santos, S. R., Ribeiro, A. A., & Matioli, L. C. (2015). HLRF–BFGS Optimization algorithm for structural reliability. *Applied Mathematical Modelling, 39*, 2025–2035. https://doi.org/10.1016/j.apm.2014.10.024
Rackwitz, R., & Flessler, B. (1978). Structural reliability under combined random load sequences. *Computers & structures, 9*, 489–494. https://doi.org/10.1016/0045-7949(78)90046-9
Ruiz, A., & Price, Y. W. (2007). Test-driven GUI development with testNG and abbot. *IEEE Software, 24*, 51–57. https://doi.org/10.1109/MS.2007.92
Santos, S. R. D., Matioli, L. C., & Beck, A. T. (2012). New optimization algorithms for structural reliability analysis. *CMES - Computer Modeling in Engineering and Sciences, 83*, 23–55. https://doi.org/10.3970/cmes.2012.083.023
Shao, X., Yi, D., Huang, Z., Zhao, H., Chen, B., & Liu, M. (2013). Basic performance of the composite deck system composed of orthotropic steel deck and ultrathin RPC layer. *Journal of Bridge Engineering, 18*, 417–428. https://doi.org/10.1061/(ASCE)BE.1943-5592.0000348
SwRI. (2011). NESSUS (ver 9.6). *Southwest Research Institute (SwRI)* Accessed: June 1, 2023 http://www.nessus.swri.org/.
Tabsh, S. W., & Nowak, A. S. (1991). Reliability of highway girder bridges. *Journal of Structural Engineering, 117*, 2372–2388. https://doi.org/10.1061/(ASCE)0733-9445(1991)117:8(2372
VanDerHorn, E., & Wang, G. (2011). *A statistical study on the material properties of shipbuilding steels, sustainable maritime transportation and exploitation of sea resources* (pp. 371–378). London: Taylor & Francis Group.
Waseem, M., & Spacone, E. (2017). Fragility curves for the typical multi-span simply supported bridges in northern Pakistan. *Structural Engineering and Mechanics, 64*, 213–223. https://doi.org/10.12989/sem.2017.64.2.213
Xin, Y., Li, J., Wang, X., & Hampson, K. (2022). Load-carrying capacity assessment of an existing highway bridge based on hybrid finite-element model updating. *Journal of Performance of Constructed Facilities, 36*, Article 04022028. https://doi.org/10.1061/(ASCE)CF.1943-5509.0001729
Yu, S. S., Kim, K., Paik, I., & Kim, J. H. (2020). Development of permit vehicle classification system for bridge evaluation in Korea. *Journal of the Korea Academia-Industrial cooperation Society, 21*, 845–856. https://doi.org/10.5762/KAIS.2020.21.12.845 (in Korean).
Zhang, K., Qi, T., Li, D., Liu, X., Xue, X., & Wu, F. (2022). Health monitoring–based assessment of continuous girder bridge reinforcement. *Journal of Performance of Constructed Facilities, 36*, Article 04022001. https://doi.org/10.1061/(ASCE)CF.1943-5509.0001685
Zhang, W. M., Zhang, X. Y., & Tian, G. M. (2022). Analytical shape-finding of the three-dimensional wind-resistant rope system of a suspension bridge. *Journal of Bridge Engineering., 27*, Article 04022086. https://doi.org/10.1061/(ASCE)BE.1943-5592.0001942
Zhang, Y., & Der Kiureghian, A. (1995). Two improved algorithms for reliability analysis. In *Proceedings of the Sixth IFIP WG7.5 on Reliability and Optimization of Structural Systems*. Boston, MA: Springer. https://doi.org/10.1007/978-0-387-34866-7_32.